

Fundamental Particle Fluidization Mechanism and Handling of Fine Particles in a Rotating Fluidized Bed

Department of Chemical Engineering, Osaka Prefecture University
Sakai, Osaka 599-8531, Japan
*E-mail: watano@chemeng.osakafu-u.ac.jp

Satoru Watano*, Hideya Nakamura, Takayuki Tokuda and Tomohiro Iwasaki

Abstract

Fluidized bed has many advantages such as high heat and mass transfer rates, temperature homogeneity and good mixing property. However, conventional fluidized bed has some limitations; operation at high gas velocity leads to slugging and there exists minimum particle size for the uniform fluidization.

Recently, a rotating fluidized bed (RFB) has attracted special interest, since it has a possibility to overcome the limitations. Due to the vessel rotation, the RFB can impart high centrifugal force to particles, leading to achieve uniform fluidization of even fine particles. The RFB also exhibits good particle mixing property with lower elutriation.

In this study, we have developed a novel rotating fluidized bed and the fundamental particle fluidization mechanism is analyzed by both experimental and numerical approaches. Handling and processing of fine particles in RFB are also discussed.

Introduction

Fine powders have become a major interest lately. New functions and high qualities attributed to fine powders are expected in many industries such as pharmaceuticals, agriculture, foods, chemicals, ceramics and electronics.

The fluidization is one of the most promising techniques for the fine powder handling. The applications have been extended to a wide variety of processes such as cracking of hydrocarbons, combustion of solid fuels/wastes and roasting of ores as chemical processing, and filtration, drying, wet granulation and coating as physical processing. This is because the fluidization exhibits excellent advantages of high heat and mass-transfer rates, temperature homogeneity and high flowability of particulate materials. However, as pointed out by Geldart in his classification map [1], powders in Group C (fine size and low density) fluidize poorly, exhibiting

channeling and other untoward effects when aerated. Therefore, development of a reliable technique to improve the fluidization of cohesive fine powders is strongly required.

So far, several devices such as vibration, mechanical agitation, sound, magnetic force, and etc. have been developed to improve the fluidization of cohesive fine powders. However, it is not easy to achieve uniform fluidization and smooth handling of fine powders, despite the use of these devices.

To overcome several limitations that the conventional fluidized beds have, we have developed a novel rotation fluidized bed system. The system basically composes of a plenum chamber and a horizontal cylindrical air distributor, which rotates around its axis of symmetry inside the chamber. We have reported that the uniform fluidization of cohesive fine powders could be easily achieved, and several unit operations such as wet granulation and film coating of fine powders were successfully conducted [2-3].

In this study, fundamental fluidization mechanism of a novel rotating fluidized bed has been analyzed by both numerical and experimental approaches. The numerical approach includes a DEM (Discrete Element Method) and a CFD (Computational Fluid Dynamics) modeling. The applications of rotating fluidized bed to handling of cohesive fine powders are also reported.

Experimental

A schematic diagram of the experimental apparatus is shown in Fig. 1. The rotating fluidized bed composes of a plenum chamber and a cylindrical air distributor (I.D.400×D100mm) made of stainless sintered mesh with 20 micron opening. The horizontal cylinder (air distributor) rotates around its axis of symmetry inside the plenum chamber. There is a stationary cylindrical metal filter (I.D.140×D100mm, opening diameter is 10 micron) inside the air distributor to retain elutriated fine powders. A binary spray nozzle mounted on the metal filter sprays binder mist (mist size is around 7 to 10 micron) onto the powder bed. A pulse air-jet nozzle is also placed inside the metal filter, which cleans up the surface of the metal filter in order to prevent clogging. An air knocker is installed outside the plenum chamber to prevent powder adhesion onto the air distributor mesh and front cover. Pressure taps are mounted on the inlet and exhaust air pipes, so that a manometer measures the pressure drop across powder beds.

Figure 2 illustrates the powder flow mechanism in the rotating fluidized bed. In a conventional fluidized bed, air distributor is horizontally mounted and powder samples are introduced onto the air distributor. Powders are lifted up by a vertical airflow (drag force and buoyancy against the gravity force). In a rotating fluidized bed, powder samples are introduced inside the air distributor and are forced to the

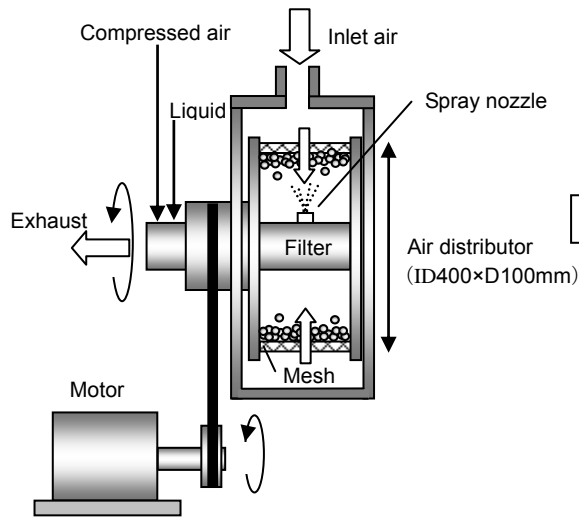


Fig.1. Schematic diagram of RFB

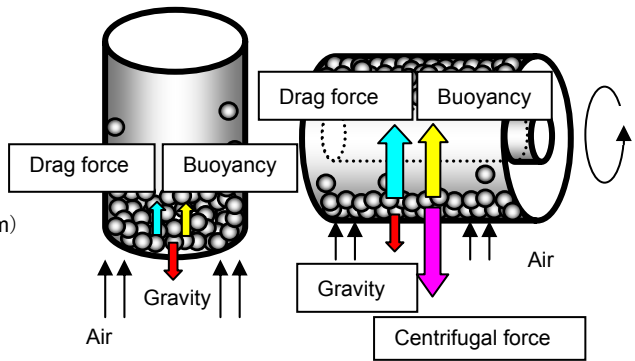


Fig.2. Particle flow mechanism in RFB

wall by a centrifugal force due to the cylinder rotation. Air flows radially inward through the air distributor, and powders are balanced by the airflow (drag force and buoyancy) and the centrifugal force. Unlike conventional fluidized beds, a rotating fluidized bed can impart high centrifugal force, which enables fine particles to behave as Geldart Group A powder [4]. The centrifugal force is incredibly large as compared to the other mechanical forces given by vibration, mechanical agitation, sound and magnetic force. This implies that the rotating fluidized bed can uniformly fluidize much finer powders than the other fluidized beds with such mechanical devices can. Theoretically, if the distributor rotates at a high enough speed and airflow increases corresponding to keep a uniform fluidization, the adhesion force between powders can be neglected as compared to the large quantity of these forces.

Numerical Modeling

Numerical simulation is one of the most useful techniques for modeling of particle fluidization. A DEM-CFD coupling model [5] has been proposed, in which individual particle and fluid motions are calculated by a discrete element method (DEM) and a computational fluid dynamics (CFD), respectively.

Modeling of fluid motion

The fluid motion is based on the locally averaged equations of continuity and motion. The fluid was assumed to be incompressible and inviscid due to the strong interaction between particle and fluid [6].

Equation of continuity:

$$\frac{\partial \varepsilon}{\partial t} + \nabla \cdot (\varepsilon \mathbf{u}) = 0 \quad (1)$$

Equation of motion:

$$\frac{\partial}{\partial t}(\varepsilon \mathbf{u}) + \nabla \cdot (\varepsilon \mathbf{u} \mathbf{u}) = -\frac{1}{\rho_f} \nabla P - \frac{\mathbf{f}_i}{\rho_f} \quad (2)$$

where ε , \mathbf{u} , P , ρ_f , \mathbf{f}_i indicate voidage, gas velocity, pressure, gas density, volumetric interaction force between particle and fluid, respectively. The fluid motion was calculated by numerically solving Eqs. (1) and (2).

Modeling of particle motion

For the modeling of particle motion, a three-dimensional discrete element method (DEM) was used. The DEM calculates the motion of each particle by integrating the Newton's second law for individual particle step by step, allowing for the external forces acting on a single particle. Equations of translational and rotational motions for individual particle are as follows [6]:

$$m \frac{d^2 \mathbf{X}}{dt^2} = \mathbf{F}_c + \mathbf{F}_d + \mathbf{F}_{cen} + \mathbf{F}_{cori} + m\mathbf{g} \quad (3)$$

$$\frac{d\boldsymbol{\omega}_p}{dt} = \frac{\mathbf{T}}{I} \quad (4)$$

where, \mathbf{X} , m , t are the position vector, mass of a particle and time, and \mathbf{F}_c , \mathbf{F}_d , \mathbf{F}_{cen} and \mathbf{F}_{cori} indicate contact, drag, centrifugal and coriolis forces, respectively. Also, \mathbf{g} , $\boldsymbol{\omega}_p$, \mathbf{T} and I show gravitational acceleration, angular velocity, moment by contact, and inertia moment, respectively. The equation of translational motion (Eq.(3)) was derived in a rotating frame. The velocity and position were calculated by integrating Eqs. (3) and (4) with respect to time step Δt .

Results and Discussion

Fundamental fluidization mechanism

Figure 3 shows the calculated and experimental results of particle fluidization behaviors in a RFB. A high-speed video camera (FASTCAM MAX, Photron CO., Ltd.) was used for visualization of actual particle fluidization behavior. The bubbling

fluidization behaviors, such as the bubble formation, eruption and particle circulation with rotational motion, could be well simulated, and these behaviors were also observed in the experimental results.

Figure 4 indicates the calculated and experimental bed pressure drop as a function of superficial gas velocity at different centrifugal accelerations. With an increase in gas velocity, the calculated bed pressure drop showed a rise to peak at minimum fluidization velocity, followed by a slight constant value with fluctuation at each centrifugal acceleration. The calculated bed pressure drop showed good agreement with the experimental one.

Fluidization regimes in a RFB were roughly classified into five regimes (Fig.4): (a) fixed bed → (b) partial fluidization → (c) partial bubbling → (d) uniform bubbling → (e) turbulent fluidization. At the low gas velocity, fluidization regime was the fixed bed, and no particle circulation was observed because the drag force acted on a particle was smaller than the centrifugal force. However, with an increase in gas velocity, the particle bed of RFB began to fluidize from inner surface of the bed (partial fluidization). This is the characteristic phenomenon in a RFB, since the gas velocity increased and the centrifugal force decreased with a decrease in radius. In this condition, particles at inner surface were fluidized while particles near at the distributor were not fluidized. When the gas velocity was much larger, the whole particle bed was fluidized completely, and the calculated bed pressure drop showed almost constant value. Also, bubbles began to generate from the top part of the vessel, and the bed height at the top was larger than at the bottom (partial bubbling). In a RFB, of which the rotational axis is horizontal, the net centrifugal acceleration was smaller at the top of the vessel than at the bottom, due to the downward gravitational force. It is thus considered that bubbling tends to occur from the top of the bed.

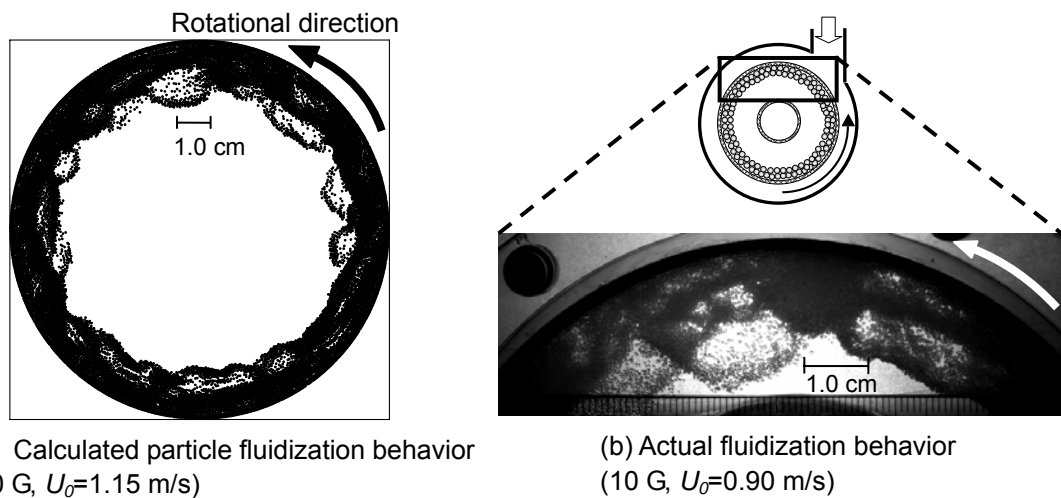


Fig. 3. Calculated and experimental results of particle fluidization behaviors in a RFB

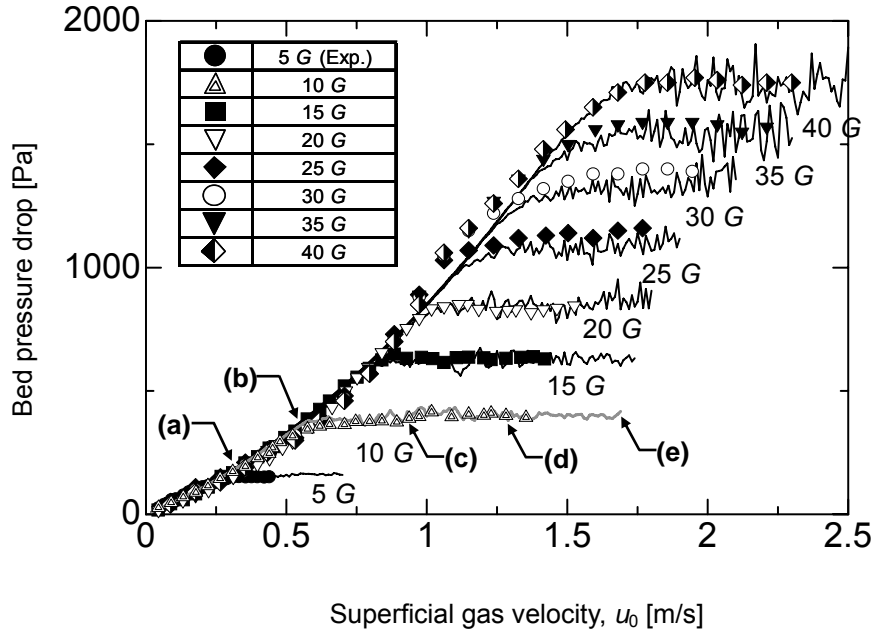


Fig. 4. Bed pressure drop vs. superficial gas velocity under different centrifugal accelerations

Mixing characteristics

We have also conducted numerical simulation to analyze particle mixing behaviors in RFB. In this study, the degree of particle mixing, M , was analyzed by both numerical simulation and experiment.

$$M = 1.0 - \frac{\sigma}{\sigma_0} \quad (5)$$

$$\sigma = \sqrt{\frac{1}{N-1} \sum_{i=1}^N (x_i - \bar{x}_c)^2} \quad (6)$$

where σ and σ_0 indicate standard deviations of fraction of tracer particles at each mixing time and initial condition, respectively. The N shows the number of sampling cells, and x_i and \bar{x}_c indicate the number fraction of tracer particles in each sampling cell and the averaged fraction in whole particle bed, respectively. In this expression, “ $M=0$ ” corresponds to completely segregated condition, and “ $M=1$ ” corresponds to completely random mixture condition.

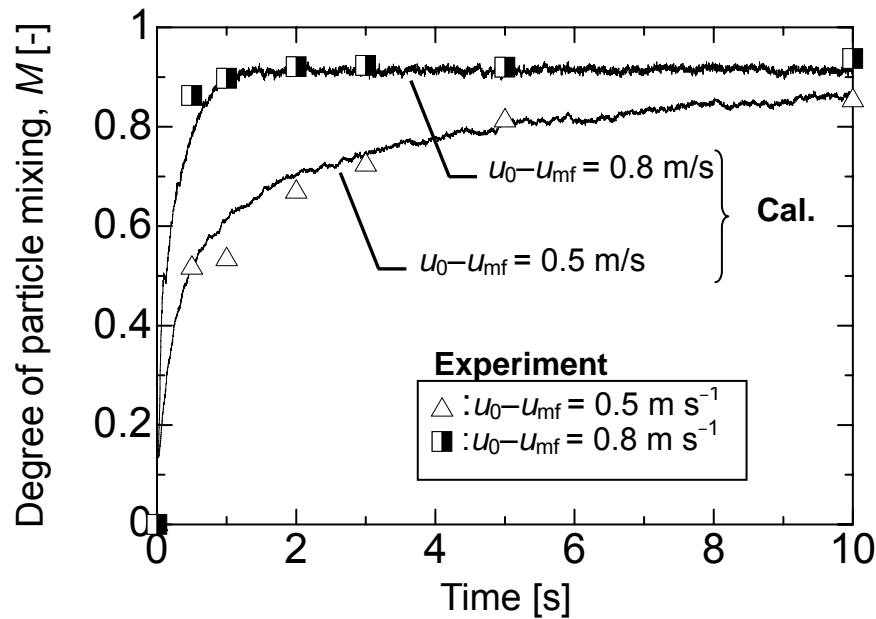


Fig. 5. Comparison between experimental and calculated results of the degree of particle mixing. ($G=20g$, Initial bed height=0.01 m)

Figure 5 shows the comparison between experimental and calculated degree of particle mixing. The calculated values on the degree of particle mixing showed good agreement with the experimental data. The numerical model developed here was considered as fully useful for the analysis of particle mixing in RFB.

Numerical simulation of film coating process

Film coating process in a RFB was also numerically analyzed based on an assumption that coating was conducted only when a particle existed within the stationary conical spray zone (Fig.6).

Figure 7 shows the temporal change in the calculated and experimental CV value (coefficient of variation) of mass distribution of the sprayed material under different gas velocities. In both cases, centrifugal acceleration was set at 10 G at each condition. With an increase in coating time, calculated and experimental CV value decreased at each gas velocity. This result implies that condition of surface coating became more uniform with an increase in coating time. Additionally, with an increase in gas velocity, calculated variation coefficient decreased, because the particle mixing became more vigorous at higher gas velocity. These tendencies of calculated results qualitatively showed good agreement with the experimental results.

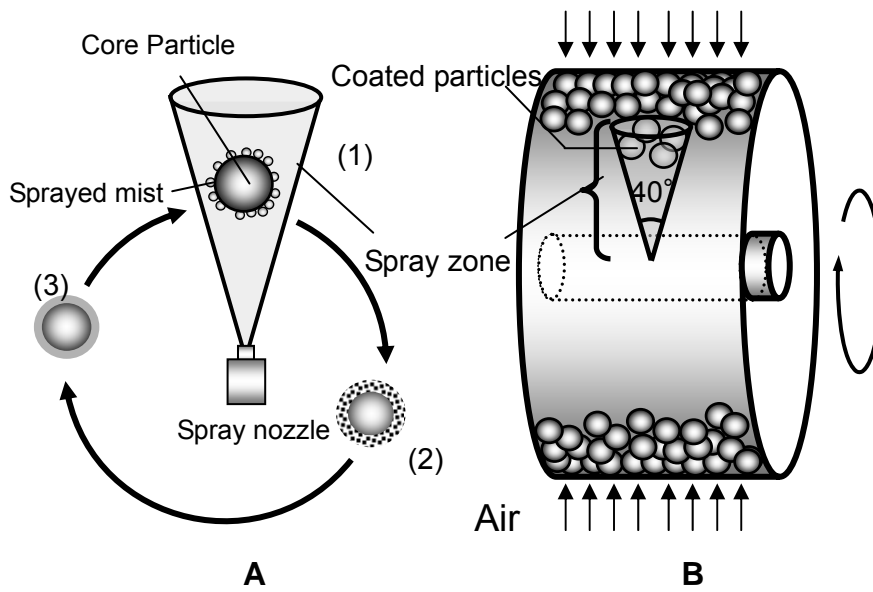


Fig.6. Model for film coating process (A) and conical spray zone (B).

(1) contact and adhesion of sprayed mist onto core particle; (2) drying and formation of film on a particle surface; and (3) re-contact and adhesion of sprayed mist onto core particle.

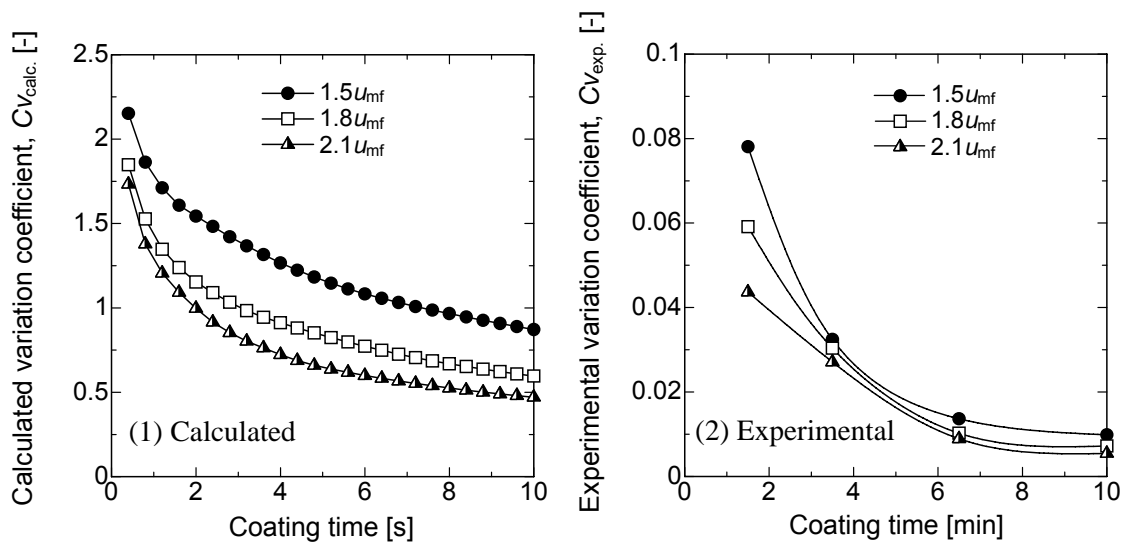


Fig. 7. Temporal change in the coating mass distribution under different gas velocities. (Centrifugal acceleration: 10 G).

Handling of fine powders

Wet granulation of nano-particle

In order to tailor the physical properties of nano-particles such as flowability, wet granulation was conducted. Hydroxypropylcellulose (HPC-L) 5% aqueous solution was sprayed onto nano-sized TiO_2 (primary size: 21 nm) particles through a binary nozzle. Fluidization air velocity was set at approximately 1.5 times as large as the minimum fluidization air velocity.

Figure 8 shows relationship between pressure drop across particle bed and air flow velocity under different centrifugal accelerations. Due to the larger radial acceleration, pressure drop increases with an increase in centrifugal acceleration.

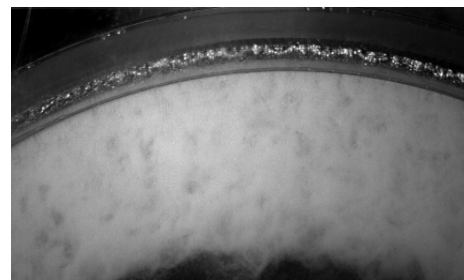
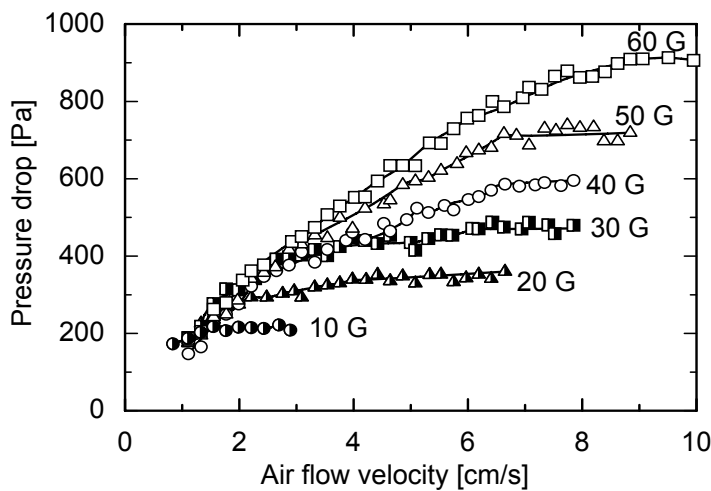


Fig.8. Fluidization behaviors of nano particle (TiO_2 : 21nm)

Fig.9. Visualization of nano fluidization (Top of the vessel, observed from front)

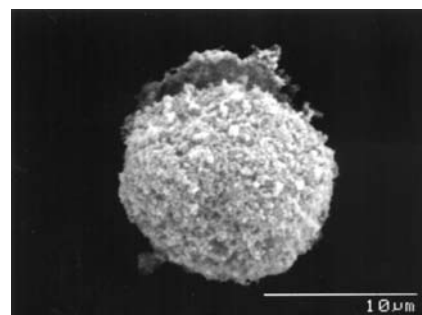
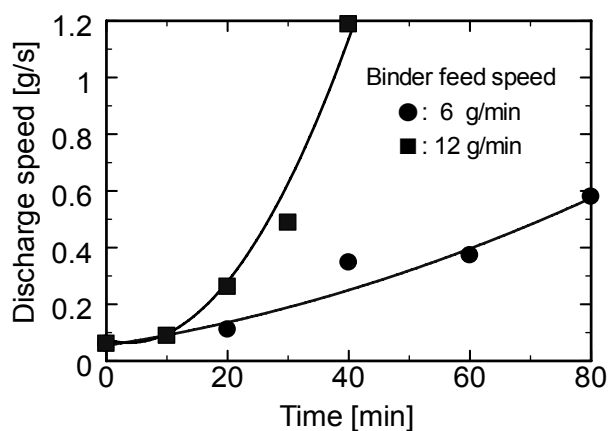


Fig.10. Discharge speed v.s. granulation time

Fig.11. SEM photograph of granule

Seen from this figure, fluidization behavior of nano-particles is almost similar to that of A-particles of Geldart's classification [1] and minimum fluidization velocity increases almost linearly with the centrifugal acceleration.

Figure 10 investigates flowability by measuring particle discharge speed from a stainless funnel. The discharge speed dramatically increased with the granulation operation time. It is because nano particles formed soft spherical granules (Fig.11) and the flowability was improved greatly. It is noteworthy that 1 g/s of the discharge speed is almost the same value that glass beads of 100-micron discharge through the same funnel. From this result, it is easily understood that the flowability of cohesive nano-particle is greatly improved by the wet granulation. The wet granulation technique of nano-particles is expected to improve physical properties of nano-particles, leading to increase the efficiency of transportation, storage, etc.

Conclusions

A numerical model based on the DEM-CFD coupling model was proposed and particle fluidization behavior in a rotating fluidized bed was simulated. The calculated fluidization behaviors, such as periodic bubbling fluidization and transition of fluidization regime were in good agreement with the ones observed by a high-speed video camera. We have also used the RFB for wet-granulation of cohesive nano powders. It was concluded that the RFB is also a reliable technique to tailor the surface properties of cohesive fine powders.

Acknowledgement

The authors wish to thank Profs. R. Pfeffer and R. N. Dave (New Jersey Institute of Technology, U.S.A.) for their useful discussions and continuous friendship.

References

- 1) Geldart, D.(1973), *Powder Technol.*, 7, 285-292.
- 2) Watano, S., Imada, Y., Hamada, K., Wakamatsu, Y., Tanabe, Y., Dave, R.N., Pfeffer, R.(2003) *Powder Technol.*, 131, 250-255.
- 3) Watano, S., Nakamura, H., Hamada, K., Wakamatsu, Y., Tanabe, Y., Dave, R.N., Pfeffer, R.(2004) *Powder Technol.*, 141, 172-176.
- 4) Qian, G.H., Bagyi, I., Burdick, I.W., Pfeffer, R., Shaw, H., Stevens, J.G.(2001) *AIChE J.*, 47, 1022-1034.
- 5) Tsuji, Y., Kawaguchi, T., Tanaka (1993) *Powder Technol.*, 77, 79-87.
- 6) Nakamura, H., Watano, S., *Powder Technol.*, in press.
- 7) Nakamura, H., Watano, S.(2006) *Studies in Surface Science and Catalysis*, 159, 505-508.
- 8) Nakamura, H., Iwasaki, T., Watano, S. (2006) *Chem. Pharm. Bull.*, 54, 839-846.